Design Rules for Discovering 2D Materials from 3D Crystals

by
Eleanor Lyons Brightbill
Collaborators: Tyler W. Farnsworth, Adam H. Woomer, Patrick C. O'Brien, Kaci L. Kuntz

Senior Honors Thesis
Chemistry
University of North Carolina at Chapel Hill

April 7th, 2016

Approved:

Abstract

Two-dimensional (2D) materials are championed as potential components for novel technologies due to the extreme change in properties that often accompanies a transition from the bulk to a quantum-confined state. While the incredible properties of existing 2D materials have been investigated for numerous applications, the current library of stable 2D materials is limited to a relatively small number of material systems, and attempts to identify novel 2D materials have found only a small subset of potential 2D material precursors. Here I present a rigorous, yet simple, set of criteria to identify 3D crystals that may be exfoliated into stable 2D sheets and apply these criteria to a database of naturally occurring layered minerals. These design rules harness two fundamental properties of crystals—Mohs hardness and melting point—to enable a rapid and effective approach to identify candidates for exfoliation. It is shown that, in layered systems, Mohs hardness is a predictor of inter-layer (out-of-plane) bond strength while melting point is a measure of intra-layer (in-plane) bond strength. This concept is demonstrated by using liquid exfoliation to produce novel 2D materials from layered minerals that have a Mohs hardness less than 3, with relative success of exfoliation (such as yield and flake size) dependent on melting point.

Introduction

The successful exfoliation of graphite into monolayer graphene produced the world's first one-atom thick, high strength super-material with incredible transport properties.[1] The result was a global explosion into graphene research, and subsequent interest in alternative 2D materials. Electronic, magnetic, optical, and mechanical properties of 2D materials have been investigated for applications in catalysis, electronics, optoelectronic and spintronic devices, sensors, high performance electrodes, and nanocomposites.[2] However, despite their promise, the current library

of stable 2D materials is limited to a relatively small number of material systems and structure types. In order to continue expanding the field of 2D materials, a clear set of criteria for exploring other 2D material candidates is needed.

While much progress has been made in exploring 2D systems, only a few crystal types are represented.[3] Previous efforts to expand the library of 2D material systems have relied on computer-based techniques. For example, Revard and Collegues created a grand-canonical evolutionary algorithm to determine the structure of novel 2D materials. The algorithm used first-principles total-energy methods to identify new low-energy (i.e. stable) 2D structures and they showed that their method worked to reproduce known 2D structures of Sn-S and C-Si.[4] However, the algorithm relies on inputs of a specific composition space. While useful, this algorithm can only find a potential structure if the atomic composition is searched, and therefore ignores the wealth of information available from naturally occurring layered minerals. Lebegue and colleagues addressed this issue by applying a filtering algorithm to the International Crystallographic Structural Database (ICSD), identifying 92 possible 2D structures from 3D precursors and verified their technique by "predicting" the known 3D layered systems of graphene and hexagonal boron nitride.[5] However, any structure that was not high-symmetry with square or hexagonal in-plane structures was automatically excluded, which eliminated a large portion of the structures within the ICSD. Since this limitation prevented a full exploration of layered minerals as potential candidates, an overall simpler, more inclusive, and generally applicable set of design rules for identifying potential 2D materials is needed.

Our design rules harness two fundamental properties of crystals, Mohs hardness and melting point, to enable a rapid and effective approach to identify candidates for exfoliation. We propose that melting point is an indication of the strength of in-plane interactions while hardness

is an indication of the strength of inter-layer interactions, suggesting that an ideal precursor for exfoliation is a material with a high melting point and low Mohs hardness value. We propose that Mohs hardness is a valid indicator of the exfoliation potential of a layered mineral, with softer minerals corresponding to weaker interlayer interactions (and higher potential of exfoliation) and harder minerals to stronger interactions. Furthermore, the high in-plane bonding strength of minerals characterized by a high melting point will likely produce large, stable 2D flakes whereas lower melting point minerals will produce flakes with smaller lateral dimensions. We validated these hypotheses by first applying a data mining approach to a set of layered minerals and separating candidates based on their Mohs hardness. With this list of candidates in hand, we then designed three key experiments to test our predictions in the laboratory. Our results indicate that, unlike previous claims, melting point is not a good predictor of exfoliation potential, but rather Mohs hardness provides a better indication as to whether a material may be exfoliated into stable 2D form.[6]

Methods

Data Mining

In order to correlate Mohs Hardness with layered structure, a random subset of 400 minerals from the American Crystal Structure Database (AMCSD) was selected, approximately 10% of the total database.[7] The AMCSD, although smaller than the ICSD, was utilized because it contains only naturally occurring structures and thus Mohs hardness values are more likely to be available. The hardness value of each of the subset minerals was determined from the available literature, most commonly from the Mineralogical Society of America's *Handbook of Mineralogy*.[8] The complete list of minerals and citations for each hardness value are provided in

Table A1 in the Appendix. Of the 400 minerals, 47 were excluded because hardness data was not available. The crystal structure of each remaining mineral was constructed in Accelrys' Materials Studio from the most recent unit cell data available in the AMCSD. A mineral was designated as layered if there existed stacks of continuous, nonintersecting surfaces across which no covalent bonds are formed.

Analysis of the 400 mineral subset served to approximate the prevalence of layered systems across the full spectrum of the Mohs hardness scale and showed that the majority of layered minerals are technically classified as softer materials (Mohs = 1 to 3). This realization helped establish a "cutoff value" of Mohs hardness that we then used to focus our search and characterization of probable layered structures (Figure 1). Once this cutoff was known, we used *webmineral.com* to provide an initial list of minerals with Mohs hardness less than or equal to three.[9] The structural parameters of these minerals were determined from the literature. Once the layered minerals were identified, hardness values were verified with secondary sources and melting points were found, if available.

Materials Studio was used to build the crystal structures of layered minerals for which unit cell information and hardness values were available. Interlayer bonding between layers was classified as either van der Waals (vdW), hydrogen (H-bond), or ionic bonding and was determined from an analysis of the chemical structure. In cases of ambiguity, the bonding type was confirmed from other sources. The Materials Studio close contacts tool was also used to determine the shortest distance between atoms on adjacent layers.

Mineral and Solvent Selection

Minerals for exfoliation were selected based on melting point, hardness, and availability. The solvents were degassed prior to use and handled under nitrogen. Solvents used for the

exfoliation of hydrogen-bonded minerals were additionally dried with molecular sieves. Since exfoliation success is largely dependent on the interaction between the mineral and the solvent, five solvents with a wide range of Hildebrand and Hansen solubility parameters were selected for the study. Each vdW mineral investigated was exfoliated in each of the 5 solvents.

Table 1. Parameters of solvents for vdW mineral exfoliations.

Solvent	**Hildebrand ($MPa^{1/2}$)**	**Hansen ($MPa^{1/2}$)**			**Surface Tension @20 °C (mN/m)**	**Boiling point (°C)**
		δ_d	δ_p	δ_h		
Chlorobenzene	19.6	19	4.3	2	33.6	131
Benzyl benzoate	21.3	20	5.1	5.2	45.95	323
N-methyl-2-pyrrolidone (NMP)	23	18	12.3	7.2	40.79	203
Isopropylalcohol (IPA)	23.6	15.8	6.1	16.4	23	82.6
Dimethylformamide (DMF)	24.9	17.4	13.7	11.3	36.7	153

2D Material Preparation

All dispersions were prepared in a nitrogen-filled glove box (O_2 < 1 ppm) to prevent oxidation of air sensitive minerals. Minerals were crushed with a mortar and pestle and 1 mg/mL solutions of each mineral were prepared in a scintillation vial that was tightly capped and wrapped with electrical tape. Each sample was sonicated for four 99-minute cycles in a Branson 5800 bath sonicator outside the glovebox, and the bath water was changed after each cycle to maintain a

temperature between 22 and 30 °C. The resulting solutions were analyzed by TEM to identify which solvents led to exfoliation, if any. The identity of thin sheets was verified by electron diffraction. Solutions of 2 mg/mL were made in the successful solvents and sonicated for 10 hours. The resulting solutions were transferred to Nalgene Oak Ridge FEP 10-mL centrifuge tubes and centrifuged at 15,000 rpm in a Sorvall RC-5B superspeed refrigerated centrifuge (rotor radius 10.7 cm). The supernatant was subsequently removed and replaced with IPA. The solvent transfer process was repeated three times to completely remove the starting solvent, and the final solutions were analyzed via TEM. The solvent transfer step was completed to reduce the presence of organics on the TEM grid and allow for shorter grid drying time. If large aggregates were observed on the TEM grid, the solutions were diluted to allow individual flakes to be imaged.

Transmission Electron Microscopy (TEM)

For imaging, 0.8-1.0 μL of solution was drop-cast onto a 300 mesh lacy carbon grid (Ted Pella) in the glovebox and allowed to dry. A JEOL 100CX II TEM was used for low resolution imaging. The TEM was operated at 100 kV accelerating voltage and had a resolution of 2 Å (lattice) and 3 Å (point to point). A charge-coupled device (CCD) camera was used to acquire all TEM images.

TEM Image Analysis

In order to improve image quality for analysis, an image averaging and background subtraction procedure was developed. Each final image used for contrast analysis is the average of 6 background-subtracted images. Background images were collected from the vacuum between the carbon grid at an intensity similar to the images.

The line profilometer tool of Gatan Digital Micrograph was used to measure the size and contrast of thin flakes, as previously described.[10] The size of flakes was determined by

approximating the flakes as simple rectangles and triangles. Contrast analysis was accomplished by computing the difference between the average of 300 pixels from both the flake surface and representative background.

Results

Mohs hardness is defined as a measure of the resistance of a mineral to a scratching deformation, and is determined from a simple scratch test between the mineral of interest and a set of 10 standard minerals.[11] For example, a mineral with hardness 3.5 can scratch Calcite (3) but not Fluorite (4). As shown in Figure 1, the prevalence of layered minerals decreases with increasing Mohs hardness. This is expected, since minerals at the high end of the hardness scale tend to be covalent network solids such as diamond with strong, rigid bonds. Layered structures as defined in this work can be more easily deformed than these structures due to the weaker bonding between layers, and thus few layered minerals have a high hardness value. At the other extreme, the standard mineral for a Mohs hardness of 1 is talc, a layered mineral. A cutoff value of 3 for Mohs Hardness was selected for further investigation (as described above) because few layered materials exist at Mohs hardness values greater than 3.

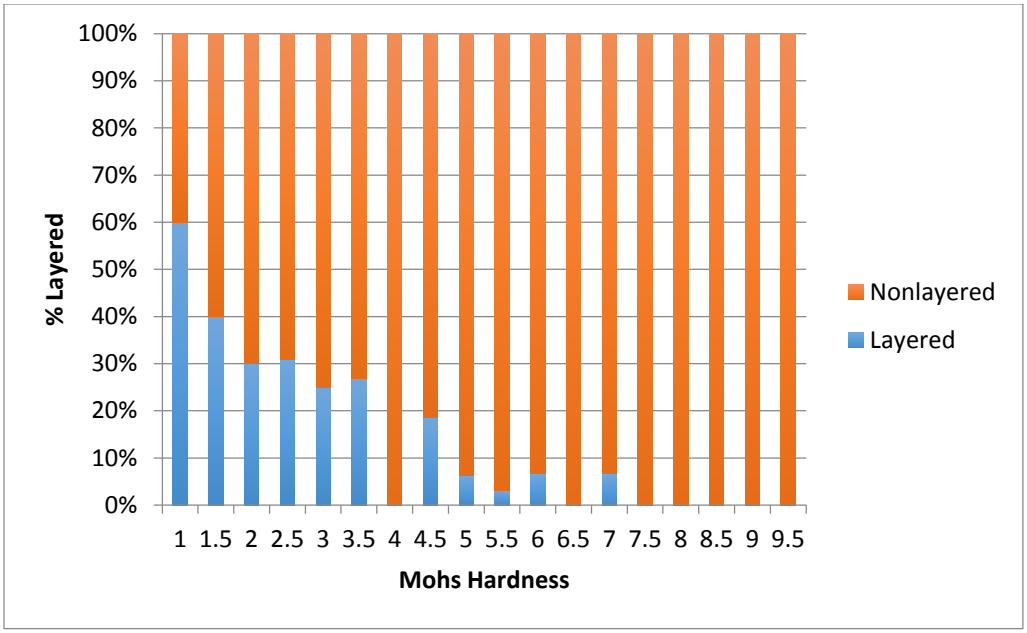


Figure 1. Prevalence of layered structures across the Mohs hardness scale from AMCSD subset.

Furthermore, the Mohs hardness of a layered structure can be used to estimate the strength of interlayer binding. Data from the layered minerals discovered from the *webmineral.com* list was used to create Figure 2 below. As shown in Figure 2 (top), the prevalence of weak interlayer bonding (vdW) decreases with higher Mohs hardness values: vdW-bonded systems comprise more than 50% of minerals with Mohs = 1 but drops to less than 10% when Mohs = 2.75. To further probe the relationship between hardness and interlayer binding strength, the interlayer distance is plotted versus Mohs hardness in Figure 2 (bottom), separated by bonding type. Here, the distance is determined as the shortest atom-to-atom contact distance between layers and is generally shorter for stronger bonding. It is clearly shown that minerals with vdW bonding are associated with larger interlayer distances than minerals with stronger interlayer bonding.

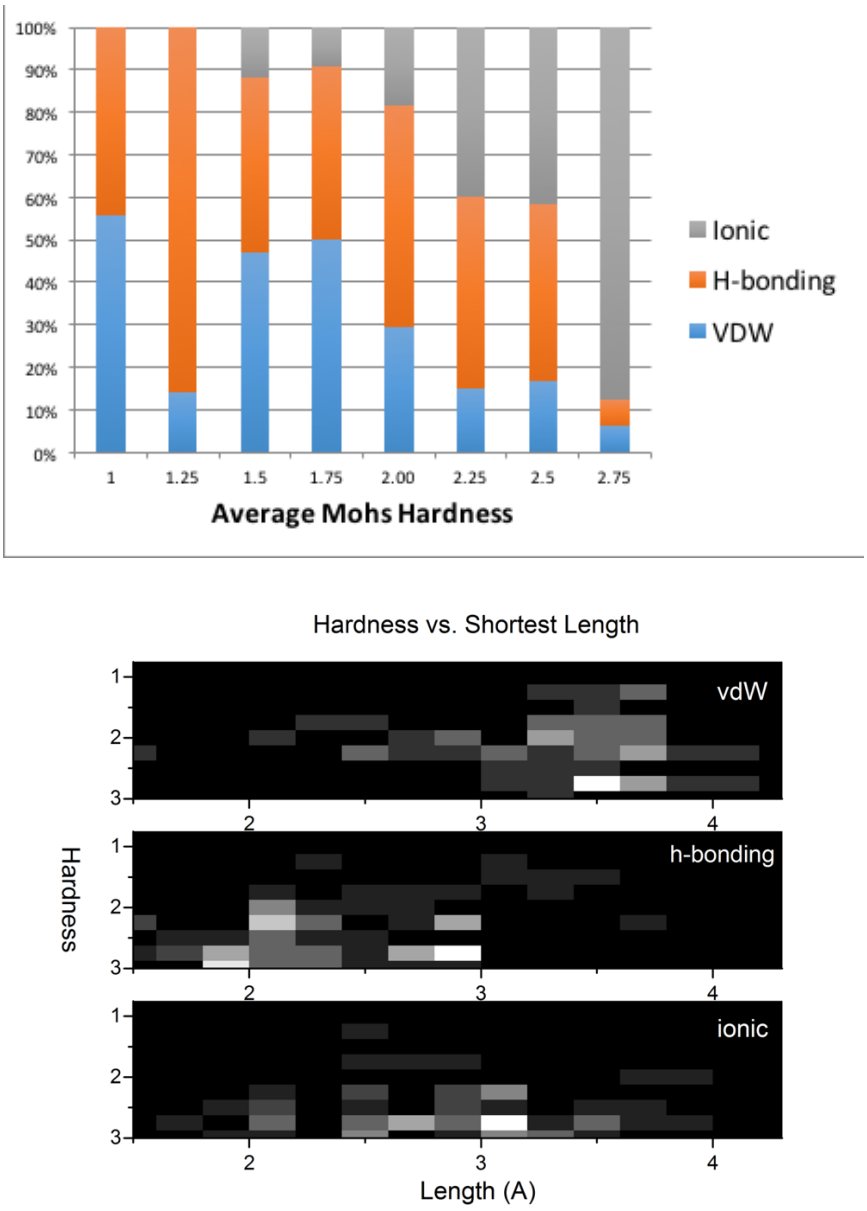


Figure 2. Top: Prevalence of interlayer bonding type by Mohs Hardness. Bottom: 3D histogram showing prevalence of hardness and layer separation by bonding type.

The melting point of a material is directly related to bond strength, and generally increases with Mohs hardness.[12] However, the 3D precursors of known 2D materials do not follow this trend. Graphite, molybdenum disulfide, and hexagonal boron nitride crystals all have much lower hardness values than would be predicted based on their melting points (4500 °C, 1185 °C, 3000 °C) due to their layered structures. While these minerals have strong in-plane bonds that result in

high melting points, the layers are held together by weak vdW forces, allowing them to slide easily relative to one another. Of the layered minerals we have identified, we find no direct correlation between hardness and melting point.

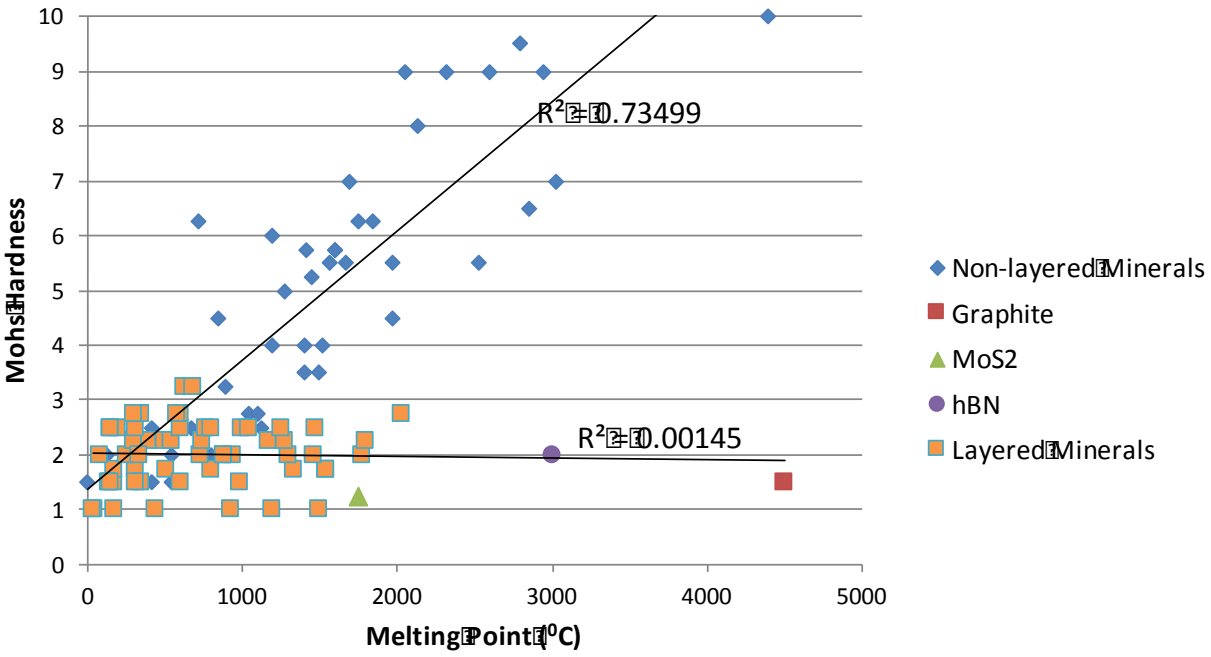


Figure 3. Mohs hardness generally correlates with melting point, but the trend does not hold for layered minerals.

From the data above, it is a reasonable hypothesis that Mohs hardness will determine how easily a layered mineral can be exfoliated due to a relationship with interlayer bonding strength. Similarly, melting point will determine the ultimate lateral size of an exfoliated flake since minerals with stronger in plane bonds should break into fewer pieces during the physical stress of liquid exfoliation. These hypotheses are confirmed with both experimental and literature data by comparing the exfoliation minerals with the same Mohs hardness but different melting points, and minerals with the same melting point but different Mohs hardness. Furthermore, it is shown that H-bond minerals without interlayer water can be exfoliated given a properly low Mohs hardness.

Experiment 1: Same Mohs hardness, different melting point

We predict that Mohs hardness is a good indicator of the ability to exfoliate stable monolayers from a bulk material. Moreover, the ability to exfoliate a layered mineral to a stable monolayer does *not* depend strictly on melting point. However, lower melting point minerals should yield flakes with smaller lateral dimensions than flakes exfoliated from higher melting point materials.

Two minerals that have not been previously exfoliatiated, Orpiment and Pyrophyllite, were selected to further support this claim. Both minerals have a Mohs hardness of 1.75, but melting points of 320 °C and 800 °C, respectively, and were exfoliated in the five solvents as described above. From this preliminary study, Orpiment was found to exfoliate best in dimethyl formamide and Pyrophyllite was found to exfoliate best in chlorobenzene. All data presented is from these two solvents. While I do show that both materials may be exfoliated in these solvents, it may be important to note that Pyrophyllite does not remain suspended in chlorobenzene while some of the Orpiment will remain in the dimethyl formamide, suggesting that the disparities in exfoliation success are even greater than presented here.

I used contrast analysis of TEM images to determine flake thickness, as previously described.[10] A histogram showing the contrast change for fifty Pyrophyllite sheets is shown below, indicating that each layer has a contrast change of approximately 20. This result is reasonable, as a monolayer of black phosphorous was determined to exhibit a contrast change of 25.[10] Similar histograms were constructed for each exfoliated mineral to determine the contrast change per layer, which was used to determine thickness.

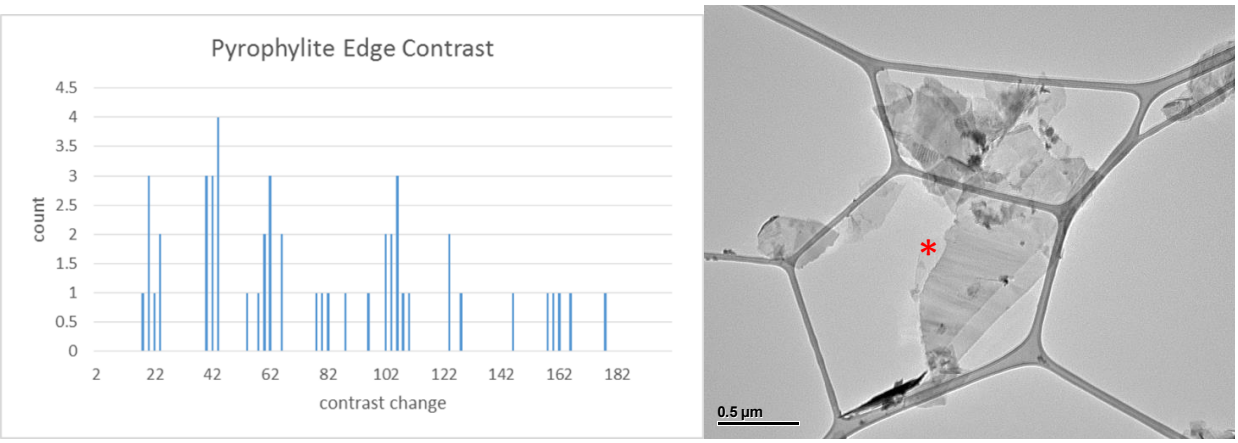


Figure 4. Left: Contrast change histogram for Pyrophyllite. Right: Red star marks a monolayer region of the flake.

Representative thin flakes of Pyrophyllite and Orpiment are shown below. Electron diffraction was used to confirm the atomic structure of the thin flakes. Qualitatively, the exfoliation of Pyrophyllite resulted in a significantly higher yield of thin flakes, while the exfoliation of Orpiment left many small, thick pieces.

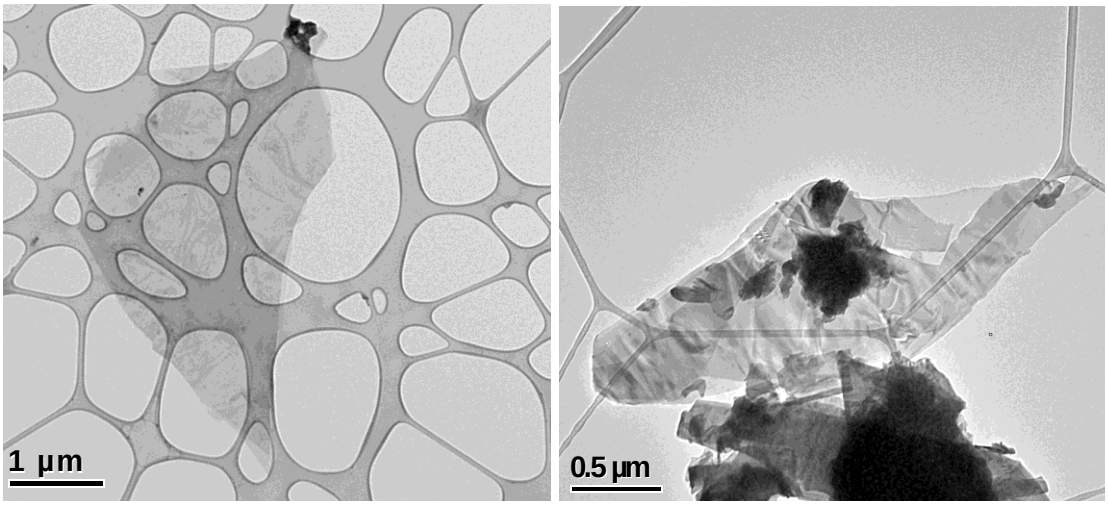


Figure 5. Thin flakes of Pyrophyllite (left) and Orpiment (right).

In order to describe the differences in flake distributions, twenty flakes of each mineral were randomly selected, excluding bulk pieces and particulate matter (smaller than 0.01 μm^2 in size). Contrast analysis was used to determine the thickness of each flake; for flakes with stepped

layers, the thickness that represented the largest area of the flake was used. The results of this analysis is shown in Table 2 below. In agreement with the hypothesis that melting point will predict lateral size, the typical area for an Orpiment flake is significantly smaller than that of Pyrophyllite while the thickness is noticeably larger. However, Orpiment was still successfully exfoliated to stable few-layer sheets despite its low melting point, just with a much lower yield.

Table 2. Thickness and surface areas of Pyrophyllite and Orpiment flakes.

Pyrophyllite		**Orpiment**	
# Layers	Area (μm^2)	# Layers	Area (μm^2)
4	2.75	7	9
2	0.23	5	0.16
4	3.30	27	0.80
7	0.72	10	0.85
10	7.60	11	0.27
3	1.20	12	0.07
6	12.60	16	0.18
6	34.60	21	0.18
6	2.90	10	4.80
5	1.30	12	2.00
5	0.18	10	9.00
8	0.19	10	1.60
5	8.10	11	1.20
4	1.50	10	1.30
8	0.17	11	5.00
2	0.20	11	7.80
13	0.15	4	0.04
1	0.03	6	1.50
2	0.01	18	0.25
6	5.60	25	0.03
Average	**4.17**	**Average**	**2.30**

In agreement with the hypothesis that melting point will predict lateral size, the typical area for an Orpiment flake is significantly smaller than that of Pyrophyllite (average thicknesses 4.17 and 2.30 μm^2, respectively). Additionally, as shown in Figure 6, most orpiment flakes were 10 or more layers, while only one of the sampled Pyrophyllite flakes was that thick. However, Orpiment

was still successfully exfoliated to stable few-layer sheets despite its low melting point, just with a much lower yield.

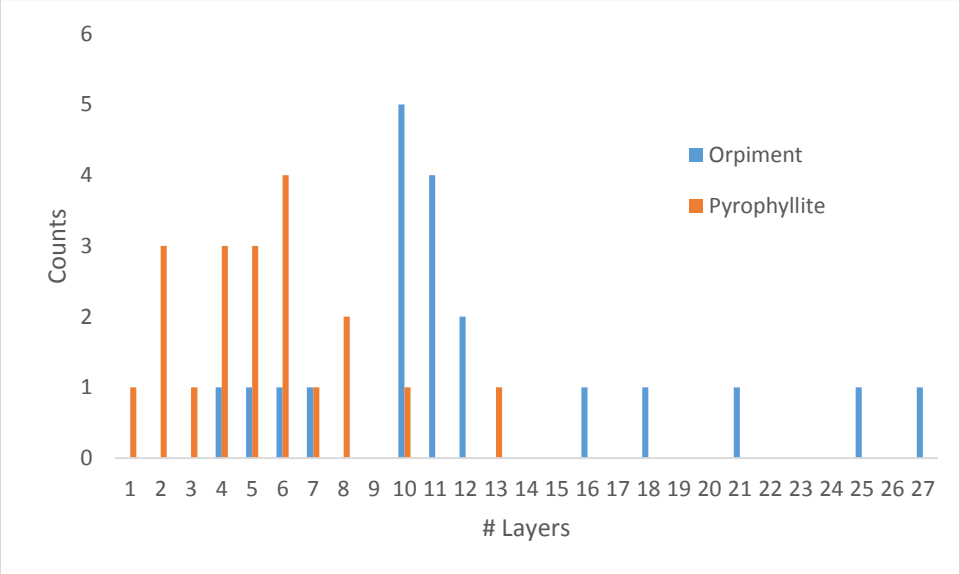


Figure 6. Thickness of Pyrophyllite and Orpiment flakes.

Experiment 2: Same melting point, but different Mohs hardness

If Mohs hardness is a measure of interlayer binding strength in layered systems, there should be a cut-off point above which minerals may no longer be exfoliated. To investigate this claim, two minerals with similar melting points (within 30 °C) but different Mohs hardness were selected. Berndtite (SnS_2) and Antimony have melting points of 600 °C and 630 °C, respectively, but Mohs hardness values of 1.5 and 3.25. Based on our predictions, we would expect Berndtite to produce stable 2D flakes while exfoliation of Antimony would result in bulk-like flakes with small lateral dimension. We found that Berndtite has previously been successfully exfoliated in a 1:4 IPA/water mixture.[13] Our own experiments demonstrated that Antimony was not able to exfoliated into 2D form, despite using solvents covering a wide range

of Hansen solubility parameters, suggesting that the interlayer interactions in Antimony are too great to be overcome by a simple liquid exfoliation protocol (Table 1).

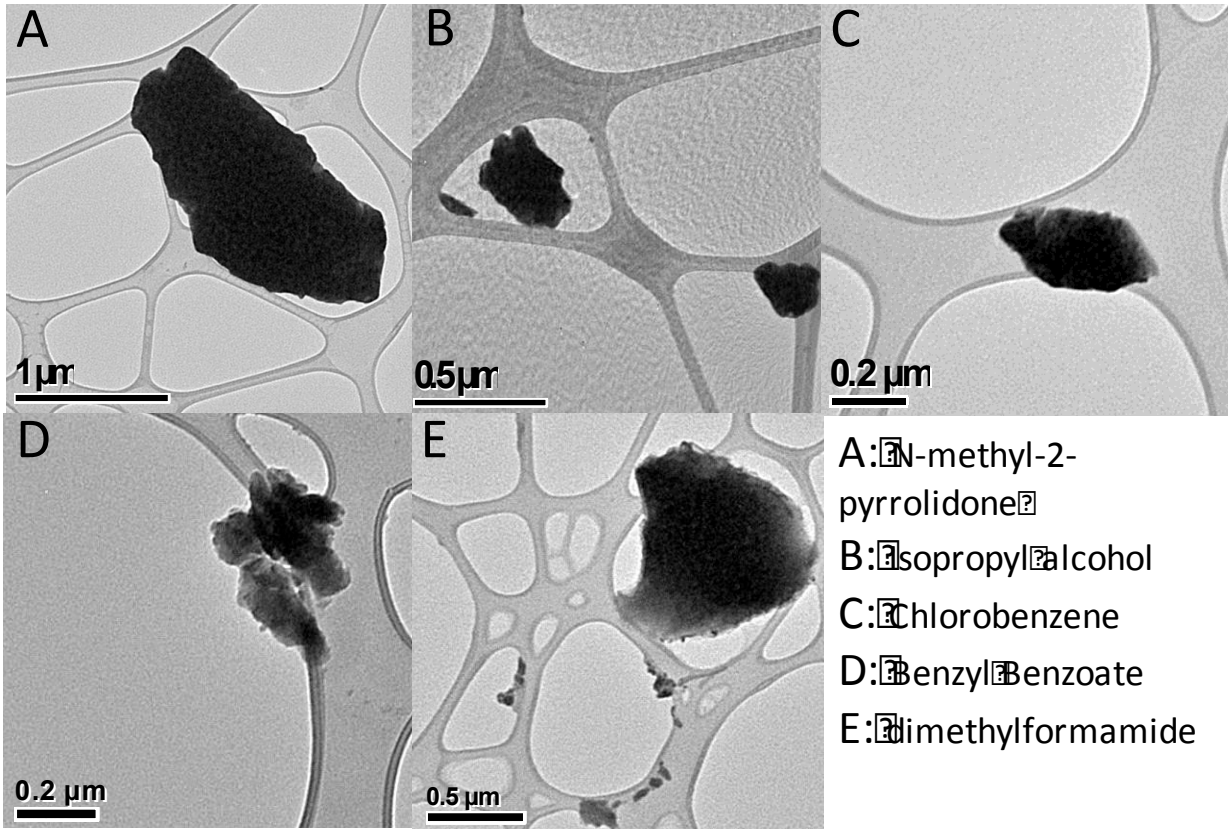


Figure 7. TEM images of Antimony from each selected solvent.

Experiment 3: Exfoliation of Hydrogen-bonded material

Although liquid exfoliation of vdW and several ionic systems has been previously demonstrated, exfoliation of minerals with interlayer hydrogen bonding (non water-based) has not been demonstrated to the best of my knowledge.[14] Several of our candidates include some degree of hydrogen bonding between the layers, often without interlayer water present in the crystal structure. Hydrogen bonds are a particularly strong dipole interaction, and therefore H-bond minerals fall higher on the Mohs scale than most vdW solids (Figure 2). However, these

minerals can, in fact, be exfoliated. We show in Figure 7 that Brucite, [$Mg(OH)_2$] (Mohs 2.75, MP=350 °C), may be successfully exfoliated in dried acetone. It is important to note that Brucite is another material with a low melting point that can be successfully exfoliated.

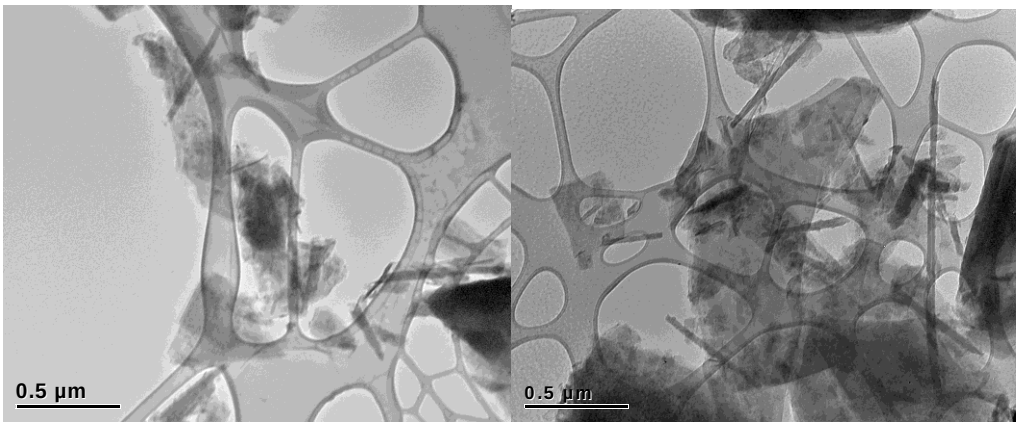


Figure 7. TEM images of Brucite exfoliated in acetone

While we successfully demonstrate that Brucite, a hydrogen bonded mineral, can be exfoliated, there are several challenges to overcome. Hydrogen bonded minerals typically have a non-negligible degree of solubility in water, and most solvents with a large hydrogen bonding Hansen parameter—and therefore most ideal for exfoliating hydrogen bonded systems—are difficult to thoroughly dry. Exfoliation of Gibbsite [$Al(OH)_3$] (Mohs 2.75, MP=2035 °C) was also attempted but was unsuccessful in acetone, methanol, ethanol, and 1-propanal, most likely due to the high solubility of the mineral in these particular solvents.

Based on our design rules, we have identified over 400 minerals that are likely candidates for being exfoliated into stable 2D flakes. A full list of identified layered candidates with appropriate Mohs hardness values is included as Table A2 in the Appendix.

Conclusions

In this work, we have demonstrated the effectiveness of using the Mohs hardness scale as a strategy for predicting novel 2D materials. Furthermore, melting point may be used to describe in-plane bonding and thus the yield and lateral size of exfoliated flakes. Thus, the most promising candidates for new 2D materials are those with a low Mohs hardness and high melting point. Specifically, we present evidence that minerals with a Mohs hardness less than three can be exfoliated given proper selection of solvent. Using an extensive data mining process and liquid exfoliation technique, we have successfully exfoliated three minerals that had never before been made in 2D form. This work signifies a huge step forward in the nanomaterial community by providing a set of design rules to expand the library of known 2D systems.

References

1. Novoselov, K. S.; Geim1, A. K. Morozov, S. V.; Jiang, D.; Zhang, Y.; Dubonos, S. V.; Grigorieva1, I. V.; Firsov, A. A. Electric Field Effect in Atomically Thin Carbon Films. *Science* **2004,** *306*, 666-669
2. Guptaa, A.; Sakthivela, T.; Seala, S. Recent development in 2D materials beyond graphene. *Progress in Materials Science* **2015**, *73*, 44-126
3. Mas-Balleste, R.; Gomez-Navarro, C.; Gomez-Herrero, J.; Zamora, F. 2D materials: to graphene and beyond. *Nanoscale* **2011**, *3*, 20-30.
4. Revard, B. C.; Tipton, W. W.; Yesypenko, A.; Hennig, R. G. Grand-canonical evolutionary algorithm for the prediction of two-dimensional materials. *Physical Review B* **2016**, *93*, 054117.
5. Lebègue, S.; Björkman, T.; Klintenberg, M.; Nieminen, R. M.; Eriksson, O. Two-Dimensional Materials from Data Filtering and Ab Initio Calculations. *Phys. Rev. X* **2013**, 3, 031002
6. Geim, A. K.; Grigorieva, I. V. Van der Waals heterostructures. *Nature* **2013**, *499*, 419-425.
7. Downs, R.T; Hall-Wallace, M. The American Mineralogist Crystal Structure Database. *American Mineralogist* **2003**, *88*, 247-250.
8. Anthony, J. W.; Bideaux, R. A.; Bladh, K. W.; Nichols, M. C. *Handbook of Mineralogy, Mineralogical Society of America, Chantilly, VA 20151-1110, USA* **2011**.
9. Barthelmy, D. Webmineral Mineralogy Database. *http://webmineral.com/* 2015.
10. Woomer, A. H.; Farnsworth, T. W.; Hu, J.; Wells, R. A.; Donley, C. L.; Warren, S. C. Phosphorene: Synthesis, Scale-Up, and Quantitative Optical Spectroscopy. *ACS Nano* **2015**, *9*, 8869–8884
11. Tabor, D. Mohs's hardness scale-a physical interpretation. *Proceedings of the Physical Society.Section B* **1954**, *67*, 249.
12. Railsback, L. B. Some fundamentals of mineralogy and geochemistry. www.gly.uga.edu/railsback 2006.
13. Shen, J.; He, Y.; Wu, J.; Gao, C.; Keyshar, K.; Zhang, X.; Yang, Y.; Ye, M.; Vajtai, R.; Lou, J.; Ajayan, P. M. Liquid Phase Exfoliation of Two-Dimensional Materials by Directly Probing and Matching Surface Tension Components *Nano Letters* **2015**, *15*, 5449–5454, DOI: 10.1021/acs.nanolett.5b01842
14. Nicolosi, V.; Chhowalla, M.; Kanatzidis, M. G.; Strano, M. S.; Coleman, J. N. Liquid Exfoliation of Layered Materials. Science 2013, 340, 1226419 DOI: 10.1126/science.1226419.
15. Kampf, A.; Downs, R.; Housley, R.; Jenkins, R.; Hyršl, J. Anorpiment, As2S3, the triclinic dimorph of orpiment. *Mineralogical Magazine* **2011**, *75*, 2857-2867.
16. Sejkora, J.; Ozdin, D.; Laufek, F.; Plasil, J.; Litochleb, J. Marrucciite, a rare Hg-sulfosalt from the Gelnica ore deposit (Slovak Republic), and its comparison with the type occurrence at Buca della Vena mine (Italy). *Journal of Geosciences* **2011**, *56*, 399-408.
17. Plášil, J.; Fejfarová, K.; Novák, M.; Dušek, M.; Škoda, R.; Hloušek, J.; Čejka, J.; Majzlan, J.; Sejkora, J.; Machovič, V. Běhounekite, U (SO4) 2 (H2O) 4, from Jáchymov (St Joachimsthal), Czech Republic: the first natural U4 sulphate. *Mineralogical Magazine* **2011**, *75*, 2739-2753.

18. Kampf, A.; Mills, S.; Rumsey, M.; Dini, M.; Birch, W.; Spratt, J.; Pluth, J.; Steele, I.; Jenkins, R.; Pinch, W. The heteropolymolybdate family: structural relations, nomenclature scheme and new species. *Mineralogical Magazine* **2012**, *76*, 1175-1207.
19. Rumsey, M.; Mills, S.; Spratt, J. Natropharmacoalumite, NaAl4 [(OH) 4 (AsO4) 3]. 4H2O, a new mineral of the pharmacosiderite supergroup and the renaming of aluminopharmacosiderite to pharmacoalumite. *Mineralogical Magazine* **2010**, *74*, 929-936.
20. Jolyon, R.; Ida, C. Mindat Minerology Database; Hudson Institute of Mineralogy. *http://www.mindat.org* 2015.
21. Pekov, I. V.; Zelenski, M. E.; Zubkova, N. V.; Ksenofontov, D. A.; Kabalov, Y. K.; Chukanov, N. V.; Yapaskurt, V. O.; Zadov, A. E.; Pushcharovsky, D. Y. Krasheninnikovite, KNa2CaMg (SO4) 3F, a new mineral from the Tolbachik volcano, Kamchatka, Russia. *Am. Mineral.* **2012**, *97*, 1788-1795.
22. Cooper, M. A.; Ball, N. A.; Hawthorne, F. C.; Paar, W. H.; Roberts, A. C.; Moffatt, E. Georgerobinsonite, Pb4 (CrO4) 2 (OH) 2FCl, a new chromate mineral from the Mammoth–St. Anthony mine, Tiger, Pinal County, Arizona: Description and crystal structure. *The Canadian Mineralogist* **2011**, *49*, 865-876.
23. Elliott, P.; Kolitsch, U.; Willis, A.; Libowitzky, E. Description and crystal structure of domerockite, Cu4 (AsO4)(AsO3OH)(OH) 3· H2O, a new mineral from the Dome Rock Mine, South Australia. *Mineralogical Magazine* **2013**, *77*, 509-522.
24. Nagashima, M.; Akasaka, M.; Minakawa, T.; Libowitzky, E.; Armbruster, T. Sursassite: Hydrogen bonding, cation order, and pumpellyite intergrowth. *Am. Mineral.* **2009**, *94*, 1440-1449.
25. Railsback, L. B. Patterns in the compositions, properties, and geochemistry of carbonate minerals. *Carbonates and Evaporites* **1999**, *14*, 1-20.
26. Makovicky, E.; Paar, W. H.; Putz, H.; Zagler, G. Dantopaite, Ag5Bi13S22, the 6P natural member of the pavonite homologous series, from Erzwies, Austria. *The Canadian Mineralogist* **2010**, *48*, 467-481.
27. Mills, S. J.; Kartashov, P. M.; Gamyanin, G. N.; Whitfield, P. S.; Kern, A.; Guerault, H.; Kampf, A. R.; Raudsepp, M. Fluorocronite, the natural analogue of β-PbF2, from the Sakha Republic, Russian Federation. *European Journal of Mineralogy* **2011**, *23*, 695-700.
28. Brugger, J.; Elliott, P.; Meisser, N.; Ansermet, S. Argandite, Mn7 (VO4) 2 (OH) 8, the V analogue of allactite from the metamorphosed Mn ores at Pipji, Turtmann Valley, Switzerland. *Am. Mineral.* **2011**, *96*, 1894-1900.
29. Brugger, J.; Meisser, N.; Ansermet, S.; Krivovichev, S. V.; Kahlenberg, V.; Belton, D.; Ryan, C. G. Leucostaurite, Pb2 [B5O9] Cl· 0.5 H2O, from the Atacama Desert: The first Pb-dominant member of the hilgardite group, and micro-determination of boron in minerals by PIGE. *Am. Mineral.* **2012**, *97*, 1206-1212.
30. Kampf, A. R. Miguelromeroite, the Mn analogue of sainfeldite, and redefinition of villyaellenite as an ordered intermediate in the sainfeldite-miguelromeroite series. *Am. Mineral.* **2009**, *94*, 1535-1540.
31. Ibrahim, K.; Inglethorpe, S. Mineral processing characteristics of natural zeolites from the Aritayn Formation of northeast Jordan. *Miner. Deposita* **1996**, *31*, 589-596.

32. Kampf, A. R.; Roberts, A. C.; Venance, K. E.; Dunning, G. E.; Walstrom, R. E. Ferroericssonite, the Fe2 analogue of Ericssonite, from eastern fresno county, California, USA. *The Canadian Mineralogist* **2011**, *49*, 587-594.
33. Pekov, I.; Zubkova, N.; Yapaskurt, V.; Belakovskiy, D.; Lykova, I.; Vigasina, M.; Sidorov, E.; Pushcharovsky, D. Y. New arsenate minerals from the Arsenatnaya fumarole, Tolbachik volcano, Kamchatka, Russia. I. Yurmarinite, Na7 (Fe3 , Mg, Cu) 4 (AsO4) 6. *Mineralogical Magazine* **2014**, *78*, 905-917.
34. Blaschko, S. D.; Chi, T.; Miller, J.; Flechner, L.; Fakra, S.; Kapahi, P.; Kahn, A.; Stoller, M. Strontium substitution for calcium in lithogenesis. *J. Urol.* **2012**, *189*.
35. Nomura, S.; Atencio, D.; Chukanov, N.; Rastsvetaeva, R.; Coutinho, J.; Karipidis, T. Manganoeudialyte, a new mineral from Poços de Caldas, Minas Gerais, Brazil. *Zapiski Vserossiiskogo Mineralogicheskogo Obshestva (Proceedings of the Russian Mineralogical Society)* **2010**, *139*, 35-47.
36. Galuskin, E. V.; Lazic, B.; Armbruster, T.; Galuskina, I. O.; Pertsev, N. N.; Gazeev, V. M.; Włodyka, R.; Dulski, M.; Dzierżanowski, P.; Zadov, A. E. Edgrewite Ca9 (SiO4) 4F2-hydroxyledgrewite Ca9 (SiO4) 4 (OH) 2, a new series of calcium humite-group minerals from altered xenoliths in the ignimbrite of Upper Chegem caldera, Northern Caucasus, Kabardino-Balkaria, Russia. *Am. Mineral.* **2012**, *97*, 1998-2006.
37. Larsen, A. O.; Kolitsch, U.; Gault, R. A.; Giester, G. Eirikite, a new mineral species of the leifite group from the Langesundsfjord district, Norway. *European Journal of Mineralogy* **2010**, *22*, 875-880.
38. Bonazzi, P.; Lepore, G. O.; Bindi, L.; Chopin, C.; Husdal, T. A.; Medenbach, O. Perbøeite-(Ce) and alnaperbøeite-(Ce), two new members of the epidote-törnebohmite polysomatic series: Chemistry, structure, dehydrogenation, and clue for a sodian epidote end-member. *Am. Mineral.* **2014**, *99*, 157-169.
39. Ockenga, E.; Yalcin, U.; Medenbach, O.; Schreyer, W. Zincohögbomite, a new mineral from eastern Aegean metabauxites. *European journal of mineralogy* **1998**, *10*, 1361-1366.
40. Tabor, D. *The hardness of metals;* Oxford university press: 2000.
41. Yusupov, R.; Stanley, C.; Welch, M.; Spratt, J.; Cressey, G.; Rumsey, M.; Seltmann, R.; Igamberdiev, E. Mavlyanovite, Mn5Si3: a new mineral species from a lamproite diatreme, Chatkal Ridge, Uzbekistan. *Mineralogical Magazine* **2009**, *73*, 43-50.
42. Novák, M.; Povondra, P.; Julie, B. Schorl-oxy-schorl to dravite-oxy-dravite tourmaline from granitic pegmatites; examples from the Moldanubicum, Czech Republic. *European Journal of Mineralogy* **2004**, *16*, 323-333.
43. Götze, J. Chemistry, textures and physical properties of quartz-geological interpretation and technical application. *Mineralogical Magazine* **2009**, *73*, 645-671.
44. Dobrzhinetskaya, L. F.; Wirth, R.; Yang, J.; Green, H. W.; Hutcheon, I. D.; Weber, P. K.; Grew, E. S. Qingsongite, natural cubic boron nitride: The first boron mineral from the Earth's mantle. *Am. Mineral.* **2014**, *99*, 764-772.

Appendix

Table A1. 349 Mineral AMCSD Subset

Mineral Name	*Structure Type*	*Mohs Hardness*	*Reference*	*Mineral Name*	*Structure Type*	*Mohs Hardness*	*Reference*
Orthominasragrite	non-layered	1	9	Corkite	non-layered	4	9
Nacrite	layered	1	9	Beaverite-(Cu)	non-layered	4	9
Burnsite	layered	1.25	9	Chabazite-K	non-layered	4	9
Epistolite	layered	1.25	9	Mushistonite	non-layered	4.25	9
Todorokite	non-layered	1.25	9	Sanmartinite	non-layered	4.25	9
Anorpiment	layered	1.5	15	Nickelschneebergite	non-layered	4.25	9
Minasragrite	non-layered	1.5	9	Yuksporite	non-layered	4.25	9
Cadmium	layered	1.5	9	Clinosafflorite	non-layered	4.25	9
Parascorodite	non-layered	1.5	9	Tancoite	non-layered	4.25	9
Nahpoite	layered	1.5	9	Phillipsite	non-layered	4.5	31
Wheatleyite	non-layered	1.5	9	Scawtite	non-layered	4.5	9
Calomel	non-layered	1.75	9	Kamiokite	non-layered	4.5	9
Halotrichite	non-layered	1.75	9	Gormanite	non-layered	4.5	9
Moschelite	non-layered	1.75	9	Ferroericssonite	layered	4.5	32
Getchellite	layered	1.75	9	Eulytine	non-layered	4.5	9
Nickelhexahydrite	non-layered	2	9	Tschortnerite	non-layered	4.5	9
Margaritasite	layered	2	9	Sarabauite	non-layered	4.5	9
Canaphite	non-layered	2	9	Jadarite	non-layered	4.5	8
Marrucciite	non-layered	2	16	Cobaltlotharmeyerite	layered	4.5	9
Sherwoodite	non-layered	2	9	Thometzekite	non-layered	4.5	9
Ellisite	non-layered	2	9	Epistilbite	non-layered	4.5	9
Behounekite	non-layered	2	17	Synadelphite	non-layered	4.5	9
Sulfur	non-layered	2	9	Punkaruaivite	non-layered	4.5	8
Beraunite	layered	2	9	Clintonite	layered	4.5	9
Rapidcreekite	layered	2	9	Brunogeierite	non-layered	4.5	9
Arsenolamprite	layered	2	9	Colemanite	non-layered	4.5	9
Henmilite	layered	2	9	Bismite	layered	4.5	9
Obradovicite-NaNa	non-layered	2	18	Yurmarinite	non-layered	4.5	33
Tincalconite	non-layered	2	9	Cupalite	non-layered	4.5	9
Hazenite	non-layered	2.25	9	Woodhouseite	non-layered	4.5	9
Montroydite	non-layered	2.25	9	Pattersonite	non-layered	4.5	9
Weibullite	non-layered	2.25	9	Mazzite-Mg	non-layered	4.5	9
Novacekite-II	non-layered	2.25	8	Stibiopalladinite	non-layered	4.5	9
Phlogopite-2O	layered	2.25	9	Scheelite	non-layered	4.5	9
Ettringite	non-layered	2.25	9	Palladseite	non-layered	4.75	9
Erniggliite	non-layered	2.5	9	Schallerite	layered	4.75	9

Neyite	non-layered	2.5	9	Davanite	non-layered	5	9
Fluorophlogopite-1M	layered	2.5	9	Gupeite	non-layered	5	9
Jouravskite	non-layered	2.5	9	Tsepinite-Na	layered	5	9
Riomarinaite	non-layered	2.5	9	Aluminocerite-(Ce)	non-layered	5	9
Aksaite	non-layered	2.5	9	Linnaeite	non-layered	5	9
Masutomilite	layered	2.5	9	Grischunite	non-layered	5	9
Natropharmacoalumite	non-layered	2.5	19	Triplite	non-layered	5	9
Rucklidgeite	layered	2.5	9	Malinkoite	non-layered	5	9
Eucairite	non-layered	2.5	9	Kostylevite	non-layered	5	9
Bamfordite	layered	2.5	9	Thomsonite-Sr	non-layered	5	9
Ulexite	layered	2.5	9	Fluorstrophite	non-layered	5	34
Tedhadleyite	layered	2.5	9	Kalininite	non-layered	5	9
Galgenbergite-(Ce)	non-layered	2.5	20	Raslakite	non-layered	5	9
Shafranovskite	non-layered	2.5	9	Poudretteite	layered	5	9
Phoenicochroite	non-layered	2.5	9	Bystrite	non-layered	5	9
Auricupride	non-layered	2.5	9	Tetranatrolite	non-layered	5	9
Lanthanite-(Ce)	layered	2.5	9	Alloclasite	non-layered	5	9
Lisiguangite	non-layered	2.5	9	Zanazziite	non-layered	5	9
Picromerite	non-layered	2.5	9	Gaitite	non-layered	5	9
Oxammite	non-layered	2.5	9	Analcime	non-layered	5	9
Cumengeite	non-layered	2.5	9	Wickenburgite	layered	5	9
Wilkmanite	non-layered	2.5	9	Brenkite	non-layered	5	8
Tungstite	layered	2.5	9	Maucherite	non-layered	5	9
Ilesite	non-layered	2.5	9	Natanite	non-layered	5	9
Lizardite-2H1	layered	2.5	9	Mesolite	non-layered	5	9
Metaswitzerite	non-layered	2.5	9	Iridarsenite	non-layered	5.25	9
Becquerelite	layered	2.5	9	Microlite	non-layered	5.25	9
Pyroaurite	layered	2.5	9	Hydroxyl-herderite	non-layered	5.25	9
Radtkeite	non-layered	2.5	9	Ilmenite	non-layered	5.25	9
Wegscheiderite	non-layered	2.75	9	Cuprorhodsite	non-layered	5.25	9
Krasheninnikovite	non-layered	2.75	21	Magnesiozippeite	non-layered	5.25	9
Fuenzalidaite	non-layered	2.75	9	Odintsovite	non-layered	5.25	9
Leonite	non-layered	2.75	9	Allabogdanite	non-layered	5.5	9
Georgerobinsonite	non-layered	2.75	22	Litidionite	non-layered	5.5	9
Roxbyite	non-layered	2.75	9	Protoferro-anthophyllite	non-layered	5.5	9
Langite	layered	2.75	9	Manganoeudialyte	non-layered	5.5	35
Heteromorphite	non-layered	2.75	9	Ferro-hornblende	non-layered	5.5	9
Cosalite	non-layered	2.75	9	Ferritaramite	non-layered	5.5	9
Fleischerite	non-layered	2.75	9	Kainosite-(Y)	non-layered	5.5	9
Kobellite	non-layered	2.75	9	Labyrinthite	non-layered	5.5	9

Krohnkite	layered	2.75	9	Bismutocolumbite	non-layered	5.5	9
Barysilite	non-layered	3	9	Clinohypersthene	non-layered	5.5	9
Nordstrandite	layered	3	9	Senegalite	non-layered	5.5	9
Domerockite	non-layered	3	23	Tivanite	non-layered	5.5	9
Nevskite	layered	3	9	Pararammelsbergite	non-layered	5.5	9
Rhodochrosite	non-layered	3	9	Zirkelite	non-layered	5.5	9
Sursassite	non-layered	3	24	Loparite	non-layered	5.5	9
Natrojarosite	non-layered	3	9	Kentbrooksite	non-layered	5.5	9
Lakebogaite	non-layered	3	9	Ferri-ottoliniite	non-layered	5.5	9
Britvinite	layered	3	9	Latrappite	non-layered	5.5	9
Connellite	non-layered	3	9	Allanite-(Ce)	non-layered	5.5	9
Agardite-(Ce)	non-layered	3	9	Grunerite	non-layered	5.5	9
Marecottite	non-layered	3	9	Marinellite	non-layered	5.5	9
Buttgenbachite	non-layered	3	9	Alluaivite	non-layered	5.5	9
Bariopharmacosiderite	non-layered	3	9	Senkevichite	non-layered	5.75	9
Chivruaiite	non-layered	3	9	Tantalaeschynite-(La)	non-layered	5.75	9
Dymkovite	layered	3	8	Hydroxyledgrewite	non-layered	5.75	36
Kambaldaite	non-layered	3	9	Zenzenite	layered	5.75	9
Paravauxite	non-layered	3	9	Wairakite	non-layered	5.75	9
Dawsonite	non-layered	3	9	Miserite	non-layered	5.75	9
Alum-(Na)	non-layered	3	9	Kristiansenite	non-layered	5.75	9
Betekhtinite	non-layered	3	9	Vicanite-(Ce)	non-layered	5.75	9
Mammothite	non-layered	3	9	Kukisvumite	non-layered	5.75	9
Thorikosite	layered	3	9	Ixiolite	non-layered	5.75	9
Chamosite	layered	3	9	Nagashimalite	non-layered	6	9
Paraershovite	non-layered	3	8	Blatterite	non-layered	6	9
Gowerite	non-layered	3	9	Fergusonite-beta-(Ce)	non-layered	6	9
Rinneite	non-layered	3	9	Ferriallanite-(Ce)	non-layered	6	9
Bobkingite	non-layered	3	9	Sarcolite	non-layered	6	9
Raite	non-layered	3	9	Eirikite	non-layered	6	37
Spencerite	layered	3	9	Periclase	non-layered	6	9
Arsenohopeite	non-layered	3	8	Fluoro-nyboite	non-layered	6	9
Ansermetite	non-layered	3	9	Niocalite	non-layered	6	9
Laurionite	non-layered	3.25	9	Fredrikssonite	non-layered	6	9
Atacamite	non-layered	3.25	9	Scandiobabingtonite	non-layered	6	9
Lindstromite	non-layered	3.25	9	Marsturite	non-layered	6	9
Astrophyllite	layered	3.25	9	Marianoite	non-layered	6	9
Reederite-(Y)	non-layered	3.25	9	Zektzerite	layered	6	9
Priceite	layered	3.25	9	Columbite-(Fe)	non-layered	6	9
Witherite	non-layered	3.25	9	Kapustinite	non-layered	6	9

Geminite	layered	3.25	9	Roaldite	non-layered	6	9
Arisite-(Ce)	non-layered	3.25	8	Cancrinite	non-layered	6	9
Rutherfordine	layered	3.25	25	Inesite	non-layered	6	9
Poitevinite	non-layered	3.3	9	Takeuchiite	non-layered	6	9
Zincolibethenite	non-layered	3.5	9	Fluoro-leakeite	non-layered	6	8
Twinnite	non-layered	3.5	9	Bikitaite	non-layered	6	9
Descloizite	non-layered	3.5	9	Epidote-(Sr)	non-layered	6.5	8
Niobophyllite	layered	3.5	9	Milarite	non-layered	6	9
Bruggenite	layered	3.5	9	Hollingworthite	non-layered	6.25	9
Catamarcaite	non-layered	3.5	9	Yuanfuliite	non-layered	6.25	9
Monetite	non-layered	3.5	9	Bazirite	non-layered	6.25	9
Hydrodresserite	non-layered	3.5	9	Magnesiocoulsonite	non-layered	6.25	9
Jonesite	non-layered	3.5	9	Glaucophane	non-layered	6.25	9
Minyulite	layered	3.5	9	Tienshanite	layered	6.25	9
Dixenite	non-layered	3.5	9	Hematite	non-layered	6.5	9
Jacutingaite	layered	3.5	8	Euxenite-(Y)	non-layered	6.5	9
Rhodesite	non-layered	3.5	9	Alnaperboeite-(Ce)	non-layered	6.5	38
Chursinite	layered	3.5	9	Berlinite	non-layered	6.5	9
Tsumebite	layered	3.5	9	Vuorelainenite	non-layered	6.5	9
Dantopaite	non-layered	3.5	26	Zincohogbomite-2N6S	non-layered	6.5	39
Calcioburbankite	non-layered	3.5	9	Belkovite	non-layered	6.5	9
Stutzite	layered	3.5	9	Jervisite	non-layered	6.5	9
Burbankite	non-layered	3.5	9	Cristobalite	non-layered	6.5	9
Akrochordite	non-layered	3.5	9	Saneroite	non-layered	6.5	9
Jensenite	non-layered	3.5	9	Zoisite	non-layered	6.5	9
Fiedlerite	non-layered	3.5	9	Tantalum	non-layered	7	40
Chalcocyanite	non-layered	3.5	9	Piemontite	non-layered	6.5	9
Fluorocronite	non-layered	3.5	27	Axinite-(Mn)	non-layered	6.75	9
Argandite	layered	3.75	28	Calcio-olivine	non-layered	6.75	9
Clinoptilolite-Na	non-layered	3.75	9	Dissakisite-(Ce)	non-layered	6.75	9
Boltwoodite	layered	3.75	9	Liberite	non-layered	7	9
Katayamalite	layered	3.75	9	Mavlyanovite	non-layered	7	41
Euchroite	non-layered	3.75	9	Paracostibite	non-layered	7	9
Pyromorphite	non-layered	3.75	9	Carbobystrite	non-layered	7	8
Wavellite	non-layered	3.75	9	Natalyite	non-layered	7	9
Cuprite	non-layered	3.75	9	Oxy-schorl	non-layered	7	42
Wurtzite	non-layered	3.75	9	Silicon	non-layered	7	9
Mckelveyite-(Y)	layered	3.75	9	Epidote	non-layered	7	9
Troilite	non-layered	3.75	9	Ominelite	non-layered	7	9
Klebelsbergite	non-layered	3.75	9	Pekovite	non-layered	7	9

Semenovite-(Ce)	non-layered	3.75	9	Carlsbergite	non-layered	7	9
Freibergite	non-layered	3.75	9	Fluor-buergerite	non-layered	7	9
Emilite	non-layered	3.75	9	Schreyerite	non-layered	7	9
Phosphosiderite	non-layered	3.75	9	Magnesiostaurolite	layered	7.25	9
Queitite	non-layered	4	9	Fluor-elbaite	non-layered	7.5	9
Vismirnovite	non-layered	4	9	Tazheranite	non-layered	7.5	9
Okanoganite-(Y)	non-layered	4	9	Stoppaniite	non-layered	7.5	9
Leucostaurite	non-layered	4	29	Euclase	non-layered	7.5	9
Lithiophosphate	non-layered	4	9	Landauite	non-layered	7.5	9
Ammoniojarosite	non-layered	4	9	Loveringite	non-layered	7.5	9
Kazakovite	non-layered	4	9	Hambergite	non-layered	7.5	9
Garavellite	non-layered	4	9	Stishovite	non-layered	7.75	9
Franciscanite	non-layered	4	9	Beryl	non-layered	7.75	9
Miguelromeroite	non-layered	4	30	Gahnite	non-layered	8	9
Gatehouseite	non-layered	4	8	Seifertite	non-layered	8.5	43
Tunisite	non-layered	4	9	Bahianite	non-layered	9	9
Algodonite	non-layered	4	9	Qingsongite	non-layered	9.5	44
Arsendescloizite	non-layered	4	9	Qusongite	non-layered	9.5	9
Bernalite	non-layered	4	9				

Table A2. Identified candidates for liquid exfoliation

Mohs Hardness	***Mineral Name***	***chemical composition***	***Mohs Hardness***	***Mineral Name***	***chemical composition***
1	Evenkite	(CH3)2(CH2)22	2.25	Haidingerite	Ca(AsO3OH)•(H2O)
1	Juanitaite	Ca10Mg4Al2Si11O39•4(H2O)	2.25	Ktenasite	(Cu,Zn)5(SO4)2(OH)6•6(H2O)
1	Molybdenite	MoS2	2.25	Pharmacolite	CaHAsO4•2(H2O)
1	Schmitterite	(UO2)TeO3	2.25	Uramphite	(NH4)(UO2)(PO4)•3(H2O)
1	Talc	Mg3Si4O10(OH)2	2.25	Muscovite	KAl2(Si3Al)O10(OH,F)2
1	Sassolite	H3BO3	2.25	Ferrisurite	(Pb,Cu)2-3(CO3)1.5-2(OH,F)0.5-1[(Fe,Al)2Si4O10(OH)2]•n(H2O)
1	Glaucocerinite	(Zn,Cu)5Al3(SO4)1.5(OH)16•9(H2O)	2.25	Chalcothallite	(Cu,Fe)6Tl2SbS4
1	Hornesite	Mg3(AsO4)2•8(H2O)	2.25	Bismoclite	BiOCl
1	Nacrite	Al2Si2O5(OH)4	2.25	Lindackerite	CuCu4(AsO4)2(AsO3OH)2•~9(H2O)

1	Meta-autunite	Ca(UO2)2(PO4)2•2-6(H2O)	2.25	Metazeunerite	Cu(UO2)2(AsO4)2•8(H2O)
1.25	Melonite	NiTe2	2.25	Phlogopite	KMg3(Si3Al)O10(F,OH)2
1.25	Droninoite	Ni3Fe+++Cl(OH)8•2H2O	2.25	Zavaritskite	BiOF
1.25	Honessite	Ni6Fe+++2(SO4)(OH)16•4(H2O)	2.25	Hydrozincite	Zn5(CO3)2(OH)6
1.25	Epistolite	(Na)2{(Na,Ti)4[Nb2(O,H2O)4Si4O14](OH,F)2}•2H2O	2.5	Vulcanite	CuTe
1.25	Tochilinite	6Fe0.9S•5(Mg,Fe++)(OH)2	2.5	Merenskyite	(Pd,Pt)(Te,Bi)2
1.25	Tochilinite	6Fe0.9S•5(Mg,Fe++)(OH)2	2.5	Moncheite	(Pt,Pd)(Te,Bi)2
1.25	Valleriite	4(Fe,Cu)S•3(Mg,Al)(OH)2	2.5	Cadmium	Cd
1.5	Rectorite	(Na,Ca)Al4(Si,Al)8O20(OH)4•2(H2O)	2.5	Urvantsevite	Pd(Bi,Pb)2
1.5	Weissbergite	TlSbS2	2.5	Mackinawite	(Fe,Ni)S0.9
1.5	Kawazulite	Bi2(Te,Se,S)3	2.5	Froodite	PdBi2
1.5	Belloite	Cu(OH)Cl	2.5	Rucklidgeite	(Bi,Pb)3Te4
1.5	Berndtite	SnS2	2.5	Chapmanite	Sb+++Fe+++2(SiO4)2(OH)
1.5	Christite	TlHgAsS3	2.5	Claudetite	As2O3
1.5	Laphamite	As2(Se,S)3	2.5	Dozyite	(Mg7Al2)(Si4Al2)O15(OH)12
1.5	Sidpietersite	Pb++4(S++++++O3S--)O2(OH)2	2.5	Tungstenite	WS2
1.5	Sinjarite	CaCl2•2(H2O)	2.5	Bamfordite	Fe+++Mo2O6(OH)3•(H2O)
1.5	Coalingite	Mg10Fe+++2(CO3)(OH)24•2(H2O)	2.5	Humberstonite	K3Na7Mg2(SO4)6(NO3)2•6(H2O)
1.5	Iriginite	(UO2)(Mo++++++2O7)•3(H2O)	2.5	Uranophane	Ca(UO2)2SiO3(OH)2•5(H2O)
1.5	Kalicinite	KHCO3	2.5	Abernathyite	K(UO2)(AsO4)•4(H2O)
1.5	Iowaite	Mg4Fe+++(OH)8OCl•2-4(H2O)	2.5	Clinobehoite	Be(OH)2
1.5	Simonkolleite	Zn5(OH)8Cl2•(H2O)	2.5	Cobaltkoritnigite	(Co,Zn)(AsO3OH)•(H2O)
1.5	Birnessite	(Na,Ca,K)x(Mn++++,Mn+++)2O4•1.5(H2O)	2.5	Alpersite	(Mg,Cu)SO4•7H2O
1.5	Koenenite	Na4Mg4Cl12•Mg5Al4(OH)22	2.5	Brushite	CaHPO4•2(H2O)
1.5	Illite *	(K,H3O)(Al,Mg,Fe)2(Si,Al)4O10[(OH)2,(H2O)]	2.5	Chalcanthite	CuSO4•5(H2O)
1.5	Straczekite	(Ca,K,Ba)(V5+,V4+)8O20•3H2O	2.5	Chesnokovite	Na2[SiO2(OH)2]•8H2O
1.75	Teallite	PbSnS2	2.5	Greenalite	(Fe++,Fe+++)2-3Si2O5(OH)4
1.75	Teallite	PbSnS2	2.5	Lanthanite-(Ce)	(Ce,La)2(CO3)3•8(H2O)
1.75	Graphite	C	2.5	Lavendulan	NaCaCu5(AsO4)4Cl•5(H2O)

1.75	Tetradymite	Bi2Te2S	2.5	Novacekite	Mg(UO2)2(AsO4)2•12(H2O)
1.75	Sylvanite	(Au,Ag)2Te4	2.5	Pentahydroborite	CaB2O(OH)6•2(H2O)
1.75	Kermesite	Sb2S2O	2.5	Poughite	Fe+++2(TeO3)2(SO4)•3(H2O)
1.75	Leiteite	ZnAs+++2O4	2.5	Pyroaurite	Mg6Fe+++2(CO3)(OH)16•4(H2O)
1.75	Ludlockite	PbFe+++4As+++10O22	2.5	Schrockingerite	NaCa3(UO2)(CO3)3(SO4)F•10(H2O)
1.75	Orpiment	As2S3	2.5	Sengierite	Cu2(UO2)2V2O8•6(H2O)
1.75	Pyrophyllite	Al2Si4O10(OH)2	2.5	Sidwillite	MoO3•2(H2O)
1.75	Vermiculite	(Mg,Fe++,Al)3(Al,Si)4O10(OH)2•4(H2O)	2.5	Sjogrenite	Mg6Fe+++2(CO3)(OH)16•4(H2O)
1.75	Vivianite	Fe++3(PO4)2•8(H2O)	2.5	Trona	Na3(CO3)(HCO3)•2(H2O)
1.75	Kuzelite	Ca4Al2.4(OH)12.8(SO4)•6(H2O)	2.5	Tungstite	WO3•(H2O)
1.75	Stichtite	Mg6Cr2(CO3)(OH)16•4(H2O)	2.5	Uramarsite	(NH4,H3O)2(UO2)2(AsO4,PO4)2•6H2O
1.75	Woodallite	Mg6Cr2(OH)16Cl2•4(H2O)	2.5	Wroewolfeite	Cu4(SO4)(OH)6•2(H2O)
1.75	Metavivianite	(Fe++3-x,Fe+++x)(PO4)2(OH)x•8-x(H2O), x=0.5	2.5	Cookeite	LiAl4(Si3Al)O10(OH)8
1.75	Dickite	Al2Si2O5(OH)4	2.5	Ungemachite	K3Na8Fe+++(SO4)6(NO3)2•6(H2O)
1.75	Kaolinite	Al2Si2O5(OH)4	2.5	Rodalquilarite	H3Fe+++2(Te++++O3)4Cl
1.75	Zdenekite	NaPbCu++5(AsO4)4Cl•5(H2O)	2.5	Schoepite	(UO2)8O2(OH)12•12(H2O)
1.75	Montmorillonite	(Na,Ca)0,3(Al,Mg)2Si4O10(OH)2•n(H2O)	2.5	Schultenite	PbHAsO4
1.75	Nontronite	Na0.3Fe+++2(Si,Al)4O10(OH)2•n(H2O)	2.5	Darapskite	Na3(SO4)(NO3)•(H2O)
1.75	Gabrielite	Tl2AgCu2As3S7	2.5	Lengenbachite	Pb6(Ag,Cu)2As4S13
2	Caresite	Fe++4Al2(OH)12CO3•3(H2O)	2.5	Franckeite	(Pb,Sn)6Fe++Sn2Sb2S14
2	Ramdohrite	Ag3Pb6Sb11S24	2.5	Hematophanite	Pb4Fe+++3O8(OH,Cl)
2	Emplectite	CuBiS2	2.5	Norrishite	K(Mn+++2Li)Si4O10(O)2
2	Arsenolamprite (arsenic)	As	2.5	Cymrite	BaAl2Si2O8•(H2O)
2	Herzenbergite	SnS	2.5	Fluorophlogopite	KMg3(AlSi3)O10F2
2	Paakkonenite	Sb2AsS2	2.5	Kenhsuite	Hg3S2Cl2

2	Vavrinite	Ni2SbTe2	2.5	Kombatite	Pb14(VO4)2O9Cl4
2	Livingstonite	HgSb4S8	2.5	Nafertisite	Na3(Fe++,Fe+++)6(Ti2Si12O34)(O,OH)7•2(H2O)
2	Cianciulliite	Mn++++(Mg,Mn++)2Zn2(OH)10•2-4(H2O)	2.5	Polylithionite	KLi2AlSi4O10(F,OH)2
2	Haydeeite	Cu3Mg(OH)6Cl2	2.5	Rossite	CaV2O6•4(H2O)
2	Koritnigite	ZnHAsO4•(H2O)	2.5	Sahlinite	Pb14(AsO4)2O9Cl4
2	Litharge	PbO	2.5	Artroeite	PbAlF3(OH)2
2	Massicot	PbO	2.5	Diaboleite	Pb2CuCl2(OH)4
2	Palmierite	(K,Na)2Pb(SO4)2	2.5	Hugelite	Pb2(UO2)3(AsO4)2(OH)4•3(H2O)
2	Tellurite	TeO2	2.5	Krausite	KFe+++(SO4)2•(H2O)
2	Erdite	NaFeS2•2(H2O)	2.5	Lamprophyllite	Na2(Sr,Ba)2Ti3(SiO4)4(OH,F)2
2	Halloysite	Al2Si2O5(OH)4	2.5	Linarite	PbCu(SO4)(OH)2
2	Namuwite	(Zn,Cu)4(SO4)(OH)6•4(H2O)	2.5	Masutomilite	K(Li,Al,Mn++)3[(Si,Al)4O10](F,OH)2
2	Chlormagalumi nite	(Mg,Fe++)4Al2(OH)12(Cl2,CO3)•2(H2O)	2.5	Oxykinoshitalite	(Ba,K)(Mg,Fe++,Ti)3(Si,Al)4O10O2
2	Brugnatellite	Mg6Fe+++(CO3)(OH)13•4(H2O)	2.5	Paragonite	NaAl2(Si3Al)O10(OH)2
2	Comblainite	Ni++6Co+++2(CO3)(OH)16•4(H2O)	2.5	Preiswerkite	NaMg2Al3Si2O10(OH)2
2	Desautelsite	Mg6Mn+++2(CO3)(OH)16•4(H2O)	2.5	Schwartzembergite	Pb++6(IO3)2O3Cl4
2	Takovite	Ni6Al2(OH)16(CO3,OH)•4(H2O)	2.5	Shirokshinite	K(NaMg2)Si4O10F2
2	Karchevskyite	[Mg18Al9(OH)54][Sr2(CO3,PO4)9(H2O,H3O)11]	2.5	Siderophyllite	KFe++2Al(Al2Si2)O10(F,OH)2
2	Meixnerite	Mg6Al2(OH)18•4(H2O)	2.5	Volkovskite	KCa4[B5O8(OH)4][B(OH)3]Cl•4(H2O)
2	Mountkeithite	(Mg,Ni)11(Fe+++,Cr)3(SO4,CO3)3.5(OH)24•11(H2O)	2.5	Devilline	CaCu4(SO4)2(OH)6•3(H2O)
2	Reevesite	Ni6Fe+++2(CO3)(OH)16•4(H2O)	2.5	Sazhinite-(Ce)	Na2Ce[Si6O14(OH)]•n(H2O), (n >= 1.5)
2	Magadiite	NaSi7O13(OH)3•4(H2O)	2.5	Caswellsilverite	NaCrS2

2	Umohoite	[(UO2)MoO4]•H2O	2.75	Hydrobiotite	[K(Mg,Fe)3(Al,Fe)Si3O10(OH,F)2]•[(Mg,Fe++,Al)3(Si,Al)4O10(OH)2•4(H2O)]
2	Annabergite	Ni3(AsO4)2•8(H2O)	2.75	Poubaite	PbBi2Se2(Te,S)2
2	Aurichalcite	(Zn,Cu)5(CO3)2(OH)6	2.75	Susannite	Pb4(SO4)(CO3)2(OH)2
2	Bazhenovite	CaS5•CaS2O3•6Ca(OH)2•20(H2O)	2.75	Kernite	Na2B4O6(OH)2•3(H2O)
2	Carboborite	Ca2Mg(CO3)2B2(OH)8•4(H2O)	2.75	Ianthinite	(UO2)•5(UO3)•10(H2O)
2	Chalcophyllite	Cu++18Al2(AsO4)3(SO4)3(OH)27•33(H2O)	2.75	Amesite	Mg2Al(SiAl)O5(OH)4
2	Gerhardtite	Cu2(NO3)(OH)3	2.75	Ankinovichite	(Ni,Zn)Al4(VO3)2(OH)12(H2O)2.5
2	Gypsum	CaSO4•2(H2O)	2.75	Bechererite	(Zn,Cu)6Zn2(OH)13[(S,Si)(O,OH)4]2
2	Hydrotalcite	Mg6Al2(CO3)(OH)16•4(H2O)	2.75	Doyleite	Al(OH)3
2	Meyerhofferite	Ca2B6O6(OH)10•2(H2O)	2.75	Gibbsite	Al(OH)3
2	Nikischerite	NaFe++6Al3(SO4)2(OH)18(H2O)12	2.75	Kottigite	Zn3(AsO4)2•8(H2O)
2	Rapidcreekite	Ca2(SO4)(CO3)•4(H2O)	2.75	Langite	Cu4(SO4)(OH)6•2(H2O)
2	Rhomboclase	(H5O2)+Fe+++(SO4)2•2(H2O)	2.75	Lithiophorite	(Al,Li)Mn++++O2(OH)2
2	Stercorite	H(NH4)Na(PO4)•4(H2O)	2.75	Murmanite	(Na)2{(Na,Ti)4[Ti2(O,H2O)4Si4O14](OH,F)2}•2H2O
2	Hummerite	KMgV+++++5O14•8(H2O)	2.75	Portlandite	Ca(OH)2
2	Inyoite	Ca2B6O6(OH)10•8(H2O)	2.75	Posnjakite	Cu4(SO4)(OH)6•(H2O)
2	Veatchite-A	Sr2B11O16(OH)5•(H2O)	2.75	Spangolite	Cu6Al(SO4)(OH)12Cl•3(H2O)
2	Glauconite	(K,Na)(Fe+++,Al,Mg)2(Si,Al)4O10(OH)2	2.75	Brucite	Mg(OH)2
2	Tobelite	(NH4,K)Al2(Si3Al)O10(OH)2	2.75	Pyrochroite	Mn(OH)2
2	Beraunite	Fe++Fe+++5(PO4)4(OH)5•4(H2O)	2.75	Gyrolite	NaCa16Si23AlO60(OH)8•64(H2O)
2	Carnotite	K2(UO2)2V2O8•3(H2O)	2.75	Thalcusite	TlCu3FeS4
2	Celadonite	K(Mg,Fe++)(Fe+++,Al)[Si4O10](OH)2	2.75	Annite	KFe++3AlSi3O10(OH,F)2

2	Scotlandite	PbSO3	2.75	Biotite *	K(Mg,Fe++)3[AlSi3O10(OH,F)2
2	Peprossiite-(Ce)	(Ce,La)(Al3O)2/3B4O10	2.75	Ershovite	Na4K3(Fe++,Mn++,Ti)2Si8O20(OH)4•5(H2O)
2	Jankovicite	Tl5Sb9(As,Sb)4S22	2.75	Kinoshitalite	(Ba,K)(Mg,Mn,Al)3Si2Al2O10(OH)2
2	Chloromenite	Cu9O2(SeO3)4Cl6	2.75	Krohnkite	Na2Cu(SO4)2•2(H2O)
2	Pyrostilpnite	Ag3SbS3	2.75	Lepidolite	K(Li,Al)3(Si,Al)4O10(F,OH)2
2	Rorisite	(Ca,Mg)FCl	2.75	Matlockite	PbFCl
2.25	Donbassite	Al2[Al2.33][Si3AlO10](OH)8	2.75	Nanpingite	Cs(Al,Mg,Fe++,Li)2(Si3Al)O10(OH,F)2
2.25	Sudovikovite	PtSe2	2.75	Phosgenite	Pb2(CO3)Cl2
2.25	Lorandite	TlAsS2	2.75	Rancieite	(Ca,Mn++)Mn++++4O9•3(H2O)
2.25	Klockmannite	CuSe	2.75	Tainiolite	KLiMg2Si4O10F2
2.25	Bobierrite	Mg3(PO4)2•8(H2O)	2.75	Tetraferriannite	K(Fe++,Mg)3(Fe+++,Al)Si3O10(OH)2
2.25	Autunite	Ca(UO2)2(PO4)2•10-12(H2O)	2.75	Wonesite	(Na,K).5(Mg,Fe,Al)3(Si,Al)4O10(OH,F)2
2.25	Borax	Na2B4O5(OH)4•8(H2O)	3	Manandonite	Li2Al4[(Si2AlB)O10](OH)8
2.25	Clinochlore	(Mg,Fe++)5Al(Si3Al)O10(OH)8	3	Sudoite	Mg2(Al,Fe+++)3Si3AlO10(OH)8